Applied Microscopy
Korean Society of Microscopy

pISSN 2287-5123 · eISSN 2287-4445
https://doi.org/10.9729/AM.2017.47.3.208

Regular Article

Structural and Morphological Changes of Co Nanoparticles and Au-10at.%Pd Thin Film Studied by in Situ Heating in a Transmission Electron Microscope

Yoon-Beom Ji, Hyun Soon Park[1,*]

Research & Development, Sung-Il Turbine Co., Ltd., Busan 46753, Korea
[1]Department of Materials Science and Engineering, Inha University, Incheon 22212, Korea

The microstructural changes in Co nanoparticles and an Au-10at.%Pd thin film have been investigated using an in situ heating holder with a micro-electro-mechanical system (MEMS). In Co nanoparticles, two phases (face-centered cubic and hexagonal close-packed crystal structures) were found to coexist at room temperature and microstructures at temperatures, higher than 1,000°C, were observed with a quick response time and significant stability. The actual temperature of each specimen was directly estimated from the changes in the lattice spacing (Bragg-peak separation). For the Au-10at.%Pd thin film, at a set temperature of 680°C, the actual temperature of the sample was estimated to be 1,020°C±123°C. Note that the specimen temperature should be carefully evaluated because of the undesired effects, i.e., the temperature non-uniformity due to the sample design of the MEMS chip, and distortion due to thermal expansion.

Key Words: In situ heating transmission electron microscope, Microelectromechanical system chip, Lattice spacing change, Morphological change, Microstructure characterization

*Correspondence to:
Park HS,
Tel: +82-32-860-7533
Fax: +82-32-862-5546
E-mail: hsparkinha@inha.ac.kr

Received August 22, 2017
Revised September 2, 2017
Accepted September 6, 2017

INTRODUCTION

Multiple environmental factors such as temperature, electric/magnetic fields, gas, and light affect the state and behavior of materials (Allard et al., 2009; Park et al., 2009; Takeo et al., 2006). An important factor that is characterized during experiments is the temperature measured inside a transmission electron microscope (TEM) (Allard et al., 2009; Asoro et al., 2013; Barwick et al., 2008; Gontard et al., 2014; Ivanov et al., 1995; Kim et al., 2015; Lee et al., 2003; Park et al., 2009; Saka et al., 2008; Takeo et al., 2006; Zhang & Su, 2009). Commercial TEM heating holders are typically based on precision-machined parts that can suffer from slow response time, drift, and instability, particularly at elevated temperatures. A micro-electro-mechanical system (MEMS) heating chip has been recently introduced into the TEM (Allard et al., 2009), allowing us to locally and precisely heat the specimen with a quick response time (maximum of approximately 10^5 K/s) and observe its behavior at a high resolution.

An important point in the temperature measurements is to determine whether the measured temperature of the samples inside the TEM is the actual temperature or the read-out temperature in the controller. Various methods are used for the temperature measurement of the samples inside the TEM. One method for measuring the actual actual sample temperature is to calibrate the measurement by observing the melting and phase transition points of the samples and comparing the read-out on the heating controller with the known values for the melting and phase transition points of the samples (Saka et al., 2008). Another method relies on the direct contact between catalyst nanoparticles and a tungsten filament with a small thermal mass, instead of using a TEM grid (Gontard et al., 2014). In yet another approach,

the sublimation kinetics from the isothermal experiments on silver nanoparticles have been used to measure the actual temperatures of the nanoparticles by considering the localized heating from the electron beam (Asoro et al., 2013).

In this work, using an in situ heating holder with the MEMS chip, the microstructural changes in the Co nanoparticles and Au-10at.%Pd thin film have been investigated with the increase in temperature. Furthermore, the actual temperature of the specimens has been estimated from the lattice-spacing changes. The original reason why we utilized the Co nanoparticles on Au-10at.%Pd thin films was the observation of magnetic phase transition of Co nanoparticles coupled with structural changes. This is our next challenge by Lorentz microscopy and/or electron holography and the results will be published somewhere in the future.

MATERIALS AND METHODS

Co nanoparticles were prepared using the pulsed wire evaporation (PWE), which is a type of the phase condensation method with an inert gas (Ivanov et al., 1995). When the high pulsed current (30 kV, 10^5 Å) passed through the Co metal wire, the wire was heated to a temperature greater than its boiling point in a considerably short time of several micro-seconds. The metal vapors condensed and formed nanoparticles (Lee et al., 2003). An Au-10at.%Pd thin film onto the MEMS chip was prepared by sputtering using an alloy target where its thickness was targeted to have 15 nm. The Co nanoparticles were dropped on the Au-10at.%Pd thin film on the SiNx electron transparent window (20 μm×5 μm×20 nm) of the MEMS chip (commercially available wildfire SiNx nanochip, DENS solutions), as illustrated in Fig. 1. As shown in Fig. 1A, the MEMS chip was equipped with the state-of-the-art four point probe to apply and measure the current and voltage through a Pt wire. Joule heating (ohmic heating) is the process wherein an electrical current is passed through the Pt wire, and the specimen temperature is therefore a function of the applied current and/

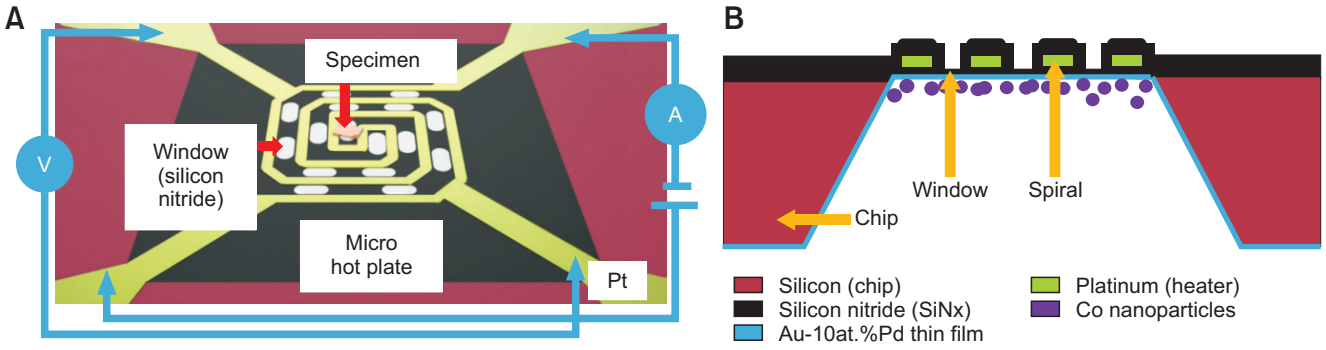

Fig. 1. Schematics showing the experimental design. (A) A specimen on the electron-transparent window (20 μm×5 μm×20 nm) of the micro-electro-mechanical system (MEMS) chip. State-of-the-art four point probe is used to apply and measure the current and voltage through the Pt wire. (B) The cross-section of the MEMS chip. Co nanoparticles are dropped on the Au-10at.%Pd thin film on the SiNx window.

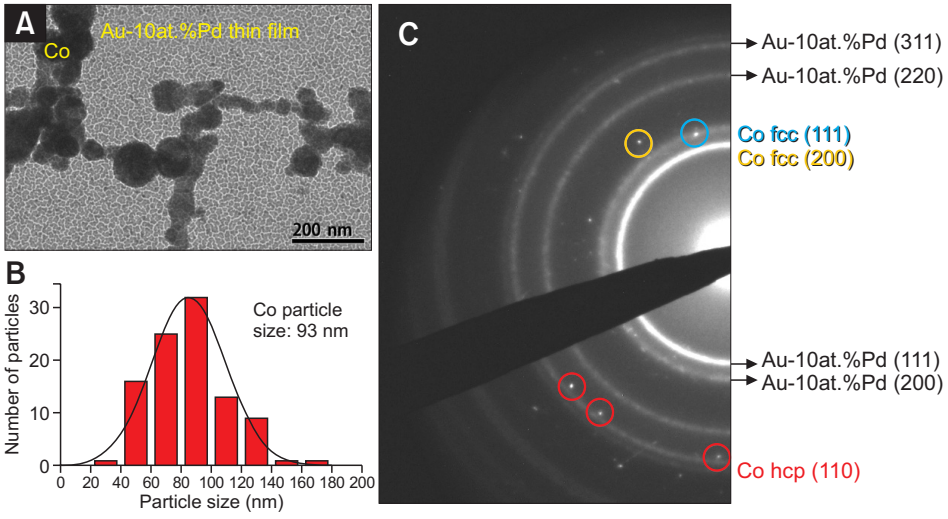

Fig. 2. Microstructures and diffraction patterns of the Co nano-particles and Au-10at.%Pd thin film. (A) Bright-field image at 23°C, showing Co nanoparticles and the Au-10at.%Pd thin film. (B) Size distribution of Co nanoparticles. (C) Selected-area electron diffraction pattern of (A). The Debye Scherrer rings and Bragg spots represent the crystallinities of the Au-10at.%Pd thin film and Co nanoparticles, respectively. Two crystal structures [face-centered cubic (fcc) and hexagonal close-packed (hcp)] of Co were observed.

or the resistance resulting from the current. An in situ heating holder (DENS solutions; Namotec., Korea) was utilized to trigger the microstructural changes in the Co nanoparticles. The microstructural and morphological changes during heating were observed inside a TEM (JEM-2010 at NanoFab.). We note that it is easier to organize a simple structure with a well-known element as a model system to calibrate the actual temperature.

RESULTS AND DISCUSSION

Fig. 2 shows the microstructures of the Co nanoparticles and the Au-10at.%Pd thin film at room temperature. The diffraction patterns of the Au-10at.%Pd thin film showed the Debye-Scherrer rings that are the signature characteristic of the polycrystalline samples. The average size of the Co nanoparticles placed on the Au-10at.%Pd thin film was measured to be 93 nm, and Co nanoparticles were found to be clustered. The Co nanoparticles were found to be both the face-centered cubic (fcc) and hexagonal close-packed (hcp)

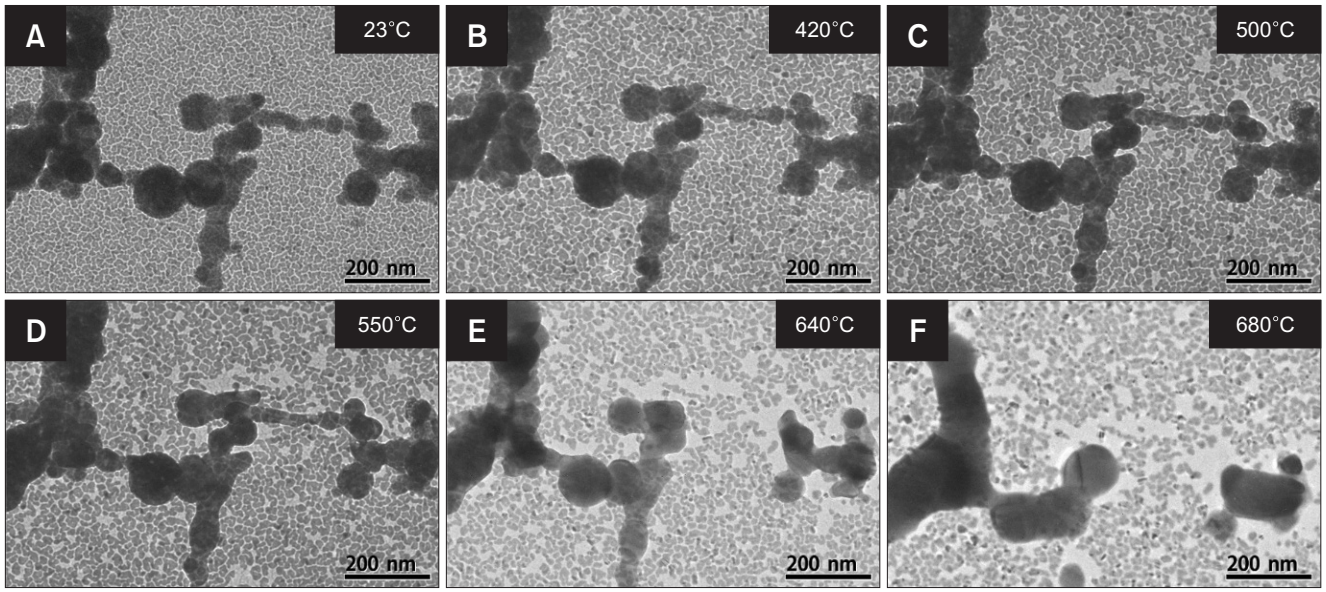

Fig. 3. Morphological changes due to in situ heating. (A-F) In situ observation of morphological changes as a function of temperature. The set temperature (input) is shown in the upper right corner of each image. Drastic changes in Co morphology appeared at 640°C. Continuous changes in the Au-10at.%Pd thin film started at 420°C Total volume of both Co and Au-10at.%Pd decreased with an increase in the temperature.

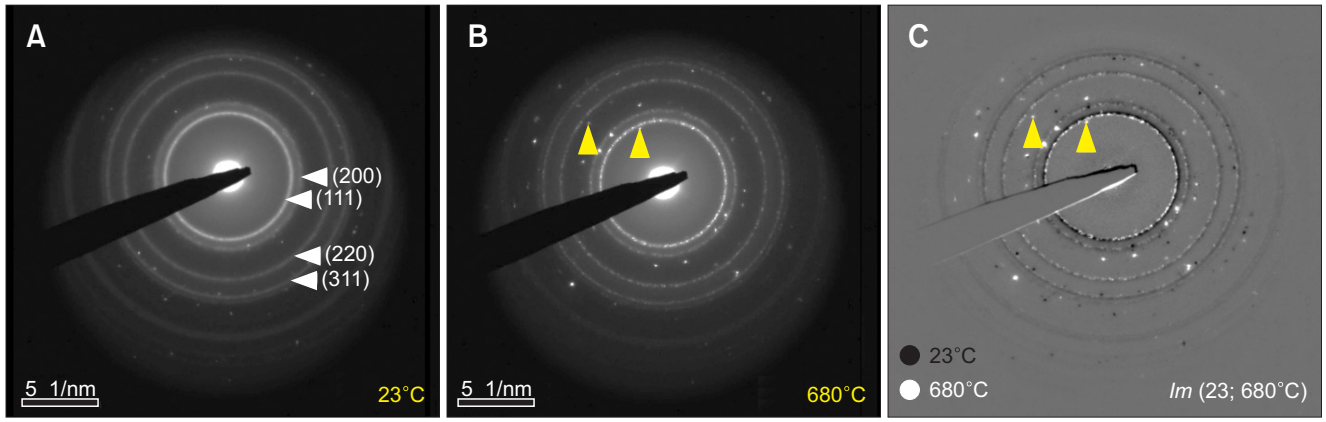

Fig. 4. Structural changes of Co particles and Au-10at.%Pd thin film at set temperatures of 23°C and 680°C. (A) Diffraction patterns obtained at 23°C. (B) Diffraction patterns obtained at 680°C. (C) A difference image, *Im* (23; 680°C), in which black and white (rings or spots) represent the crystal structures at 23°C and 680°C, respectively. In the image of *Im* (23; 680°C), the difference in the Debye Scherrer rings results from lattice expansion. The Bragg spots indicated by yellow arrow-heads newly appeared at 680°C, and are indexed by CoO.

crystal structures, which were indicated by the yellow and red circles, respectively. It is known that the hcp structure of Co is stable at room temperature and the phase transition temperature between the hcp and fcc structures is 450°C (Bao et al., 2005; Matveev et al., 2006; Yoo et al., 1998). The presence of the high-temperature phase (fcc) at room temperature is assumed to be due to the incomplete transformation of Co prepared by using the PWE method. In other words, Co transformed (from hcp to fcc) during heating up to the boiling point was rapidly cooled to room temperature and only an incomplete transformation to the more stable low-temperature phase was achieved due to rapid cooling.

The morphological changes of both the Co nanoparticles and the Au-10at.%Pd thin film were observed with an increase in the specimen temperature, as shown in Fig. 3. Note that the temperatures indicated in each image are not the actual temperatures but rather the set (input) temperatures in the controller. While drastic changes in the morphology of Co nanoparticles appeared at 640°C, the microstructures of the Au-10at.%Pd thin film continuously changed from 420°C to 680°C. Furthermore, the total number of electrons transmitted through the specimens should be considered, i.e., the number of electrons measured at 680°C was found to be approximately 49% larger than that of electrons measured at 23°C, indicating that more electrons were transmitted. Therefore, we believe that at 680°C, the total volume of both specimens decreased due to melting and/or sublimation.

Fig. 4 shows the structural changes of both specimens with increasing temperature. The Bragg spots and ring patterns in Fig. 4A and B represent the crystallinities of the Co nanoparticles and the Au-10at.%Pd thin film, respectively. Fig. 4C is an image showing the difference between the images obtained at 23°C and 680°C, *Im* (23; 680°C). In the image of *Im* (23; 680°C) the black and the white (rings or spots)

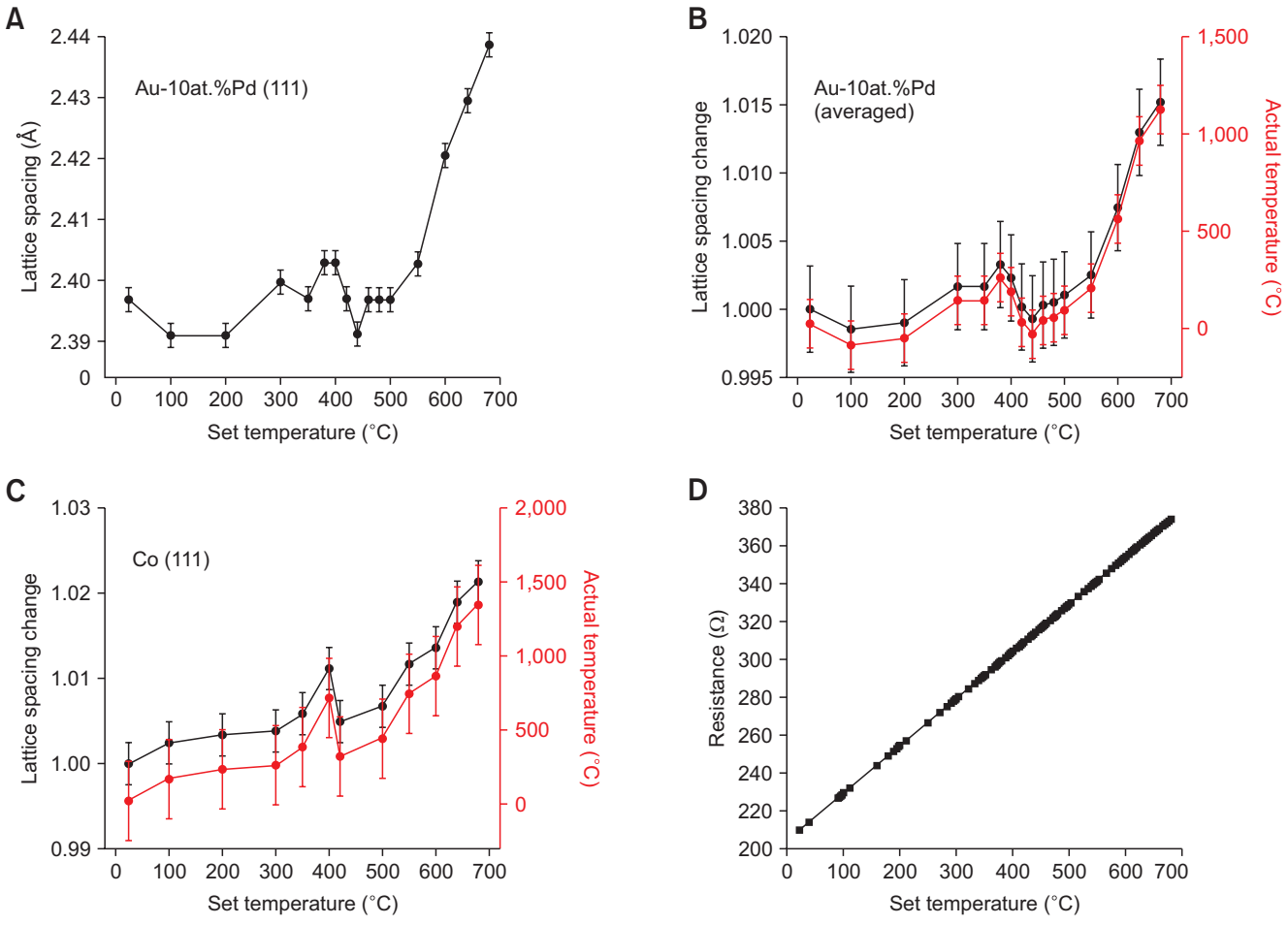

Fig. 5. Actual specimen temperatures estimated from the lattice-spacing changes by in situ heating. (A) The lattice-spacing changes of (111) planes in the Au-10at.%Pd thin film with an increase in the set temperature. (B) The lattice-spacing change averaged from three representative planes (111), (220), and (311) in the Au-10at.%Pd thin film. (C) Changes in the lattice-spacing and actual temperature of the fcc (111) (colored in red). In Fig. 5B and C, the actual temperatures (colored in red) of the two specimens were directly estimated from the lattice-spacing change and the coefficient of linear thermal expansion ($\Delta L/L=\alpha\Delta T$). (D) Resistance change as a function of the set temperature.

indicate the crystal structures at 23°C and 680°C, respectively. For example, in Fig. 4C, the white rings (at 680°C) are found inside the black rings (at 23°C); this is directly attributed to the lattice thermal expansion. We found new Bragg spots indicated by yellow arrowheads in Fig. 4B and C, which were indexed by the (111) spacing of 2.63 Å and (220) spacing of 1.51 Å of CoO, respectively (Seo et al., 2005). From the measurements of the lattice spacing in diffraction patterns, we can determine the actual temperature of the specimens in the TEM, rather than relying on the set (input) temperature in the heating controller. In Fig. 4C, the (111) lattice spacing of Au-10at.%Pd was measured as 2.396 Å at 23°C and 2.438 Å at 680°C with an error of ±0.005 Å, resulting in an lateral lattice expansion change of 1.7at.% (0.042 Å). In the report by Barwick et al. (2008), the change of averaged Bragg peak separation of 0.043 at.% in Au thin film has been measured by ultrafast electron microscopy, which gives a lateral lattice constant change of 0.17 pm (ΔT=125 K).

The lattice-spacing changes in both specimens are depicted as a function of temperature in Fig. 5. Fig. 5A shows the lattice-spacing changes and actual temperature of the (111) plane in the Au-10at.%Pd thin film with an increase in the set temperature. For quantitative analysis, the lattice-spacing change of three representative planes (111), (220), and (311) in the Au-10at.%Pd thin film was averaged. Fig. 5C shows the change in the fcc (111) lattice spacing and the deduced actual temperature of the Co nanoparticles. In Fig. 5B and C, the actual temperatures αT (colored in red) of the two specimens were directly estimated from the lattice spacing change (ΔL/L) and the thermal expansion coefficient α. For example, based on a value α of Au-10at.% Pd (approximately 15.0×10^{-6}/°C at 650°C) (Okamoto & Massalski, 1985), a lattice expansion change of 1.7at.% at the set temperatures of 23°C and 680°C directly yields the temperature change ΔT of 1,020°C±123°C (ΔL/L=αΔT). In the case of the Co nanoparticles (approximately 16.1×10^{-6}/°C at 650°C), ΔT at the set temperatures of 23°C and 680°C was estimated to be 1,327°C±150°C. Fig. 5D shows the relation between the resistance and the temperature monitored in the, along with the linear change. The differences between the actual temperature changes and ohmic changes as a function of temperature are shown in Fig. 5B-D. These results are discussed below.

Note that significant differences were observed between the set and actual temperatures of each specimen. Fig. 5D shows the set temperature dependence of the resistance, resulting from the applied current. The resistance exhibits a linear relation with the set temperature, as shown by fitting with a slope of 0.25 Ω/°C. It is worth noting that the lattice-spacing change of each specimen does not actually exhibit a linear relation. Furthermore, the lattice expansion dependences on the temperature of the two specimens, i.e., film and particle, appear to be different from each other. This may be due to the complicated effects that are related to the specimen dimensions in free space, thermal properties (e.g., conductivity, expansion coefficient, and resistivity), and contact area with the heating source as well as the SiNx membrane. Nevertheless, it is reasonable to argue that the set temperature does not completely agree with the actual temperature of the specimen, which can be determined by observing the lattice expansion changes.

Next, we discuss the morphological and structural changes. The melting and/or the sublimation of both specimens were observed as shown in the microstructural changes of Fig. 3. The islands in the Au-10at.%Pd film started to disappear from 420°C (Fig. 3B), which is attributed to sublimation. In contrast, the Co nanoparticles changed in shape and size at 640°C (Fig. 3E) via melting and/or sublimation. Based on the melting points of Au-10at.%Pd (1,200°C) and Co (1,495°C), we consider that the microstructural changes of each specimen are attributed to both the size effect and the vapor pressure dependence of the metals on the temperature. Asoro et al. (2013) reported that the sublimation temperatures were found to decrease with a decrease in the Ag particle size (5~50 nm). Zhang & Su (2009) reported that the vacuum pressure of approximately 10^{-7} Torr inside the TEM could affect the sublimation temperature depending on the melting temperature of various elements (Cu, Au, Ni, Mo), in which the sublimation of Cu occurred at approximately 660°C. However, they did not measure the actual temperature of the specimen. In our observations, the actual temperature of the specimens was estimated by directly measuring the lattice-spacing change.

CONCLUSIONS

We observed and analyzed the microstructural changes of the TEM samples (particle and thin film) as a function of temperature using an in situ heating holder with the MEMS chip. By monitoring the diffraction patterns, the actual temperatures of the samples were estimated, based on the lattice-spacing change and the thermal expansion coefficient of the samples. Even though multiple factors such as the thermal properties of materials, sample dimensions, and contact area with the heating source, make it difficult to measure the actual temperature of the samples, the actual temperatures of the samples can be estimated by directly observing the lattice-spacing change as a function of temperature. The proposed method is expected to be used for the characterization and control of the temperature of materials in real time.

CONFLICT OF INTEREST

No potential conflict of interest relevant to this article was reported.

ACKNOWLEDGMENTS

This study was supported by Inha University Research Grant (INHA-55432).

REFERENCES

Allard L F, Bigelow W C, Jose-Yacaman M, Nackashi D P, Damiano J, and Mick S E (2009) A new MEMS-based system for ultra-high-resolution imaging at elevated temperature. *Microscopy Research and Technique* **72**, 208-215.

Asoro M A, Kovar D, and Ferreira P J (2013) In-situ transmission electron microscopy observation of sublimation in silver nanoparticles. *J. ACS Nano.* **7**, 7844-7852.

Bao Y, Beermanm M, Pakhomov A B, and Krishnan K M (2005) Controlled crystalline structure and surface stability of cobalt nanocrystals. *J. Phys. Chem. B* **109**, 7220-7222.

Barwick B, Park H S, Kwon O H, Baskin J S, and Zewail A H (2008) 4D imaging of transient structures and morphologies in ultrafast electron microscopy. *Science* **322**, 1227-1231.

Gontard L C, Dunin-Borkowski R E, Fernandez F, Ozkaya D, and Kasama T (2014) Tomographic heating holder for in situ TEM: Study of Pt/C and PtPd/Al203 catalysts as a function of temperature. *Microsc. Microanal.* **20**, 982-990.

Ivanov V, Kotov Y A, and Samatov O H (1995) Synthesis and dynamic compaction of ceramic nano powders by techniques based on electric pulsed power. *Nanostructured Materials* **6**, 287-290.

Kim T H, Bae J H, Lee J W, Shin K, Lee J H, Kim M Y, and Yang C W (2015) Temperature calibration of a specimen-heating holder for transmission electron microscopy. *Appl. Microsc.* **2**, 95-100.

Lee G H, Park J H, Rhee C K, and Kim W W (2003) Fabrication of Al nano powders by pulsed wire evaporation (PWE) method. *J. Ind. Eng. Chem.* **9**, 71-75.

Matveev V V, Baranov D A, Yurkov G Y, Akatiev N G, Dotsenko I P, and Gubin S P (2006) Cobalt nanoparticles with preferential hcp structure: a confirmation by X-ray diffraction and NMR. *Chemical Physics Letters* **422**, 402-405.

Okamoto H and Massalski T B (1985) The Au-Pd (Gold-Palladium) system. *Bulletin of Alloy Phase Diagrams* **6**, 229-235.

Park H S, Baskin J S, Barwick B, Kwon O H, and Zewail A H (2009) 4D ultrafast electron microscopy: imaging of atomic motions, acoustic resonances, and moire fringe dynamics. *Ultramicroscopy* **110**, 7-19.

Saka H, Kamino T, Arai S, and Sasaki K (2008) In situ heating transmission elecctron microscopy. *J. MRS Bulletin* **33**, 93-100.

Seo W S, Shim J H, Oh S J, Lee E K, Hur N H, and Park J T (2005) Phase-and size-controlled synthesis of hexagonal and cubic CoO nanocrystals. *J. Am. Chrm. Soc.* **127**, 6188-6189.

Takeo K, Toshie Y, Mitsuru K, Akira W, and Yasuhira N (2006) Development of a specimen heating holder with an evaporator and gas injector and its application for catalyst. *Journal of Electron Microscopy* **55**, 245-252.

Yoo C, Söderlind P, and Cynn H (1998) The phase diagram of cobalt at high pressure and temperature: the stability of γ(fcc)-cobalt and new ε'(dhcp)-cobalt. *J. Phys.: Condens. Matter.* **10**, 311-318.

Zhang Z and Su D (2009) Behavior of TEM metal grids during in-situ heating experiment. *Ultramicroscopy* **109**, 766-774.